# **Bioinspiration & Biomimetics**



RECEIVED
21 December 2021

REVISED 30 May 2022

ACCEPTED FOR PUBLICATION
1 June 2022

PUBLISHED 13 July 2022 PAPER

# Branching pattern of flexible trees for environmental load mitigation

Oluwafemi Ojo and Kourosh Shoele\*

Department of Mechanical Engineering, Joint College of Engineering, Florida A & M University-Florida State University, Tallahassee, FL, United States of America

\* Author to whom any correspondence should be addressed.

E-mail: kshoele@eng.famu.fsu.edu

Keywords: flexible, fluid structure interaction, tree biomechanics, fractal structure

#### Abstract

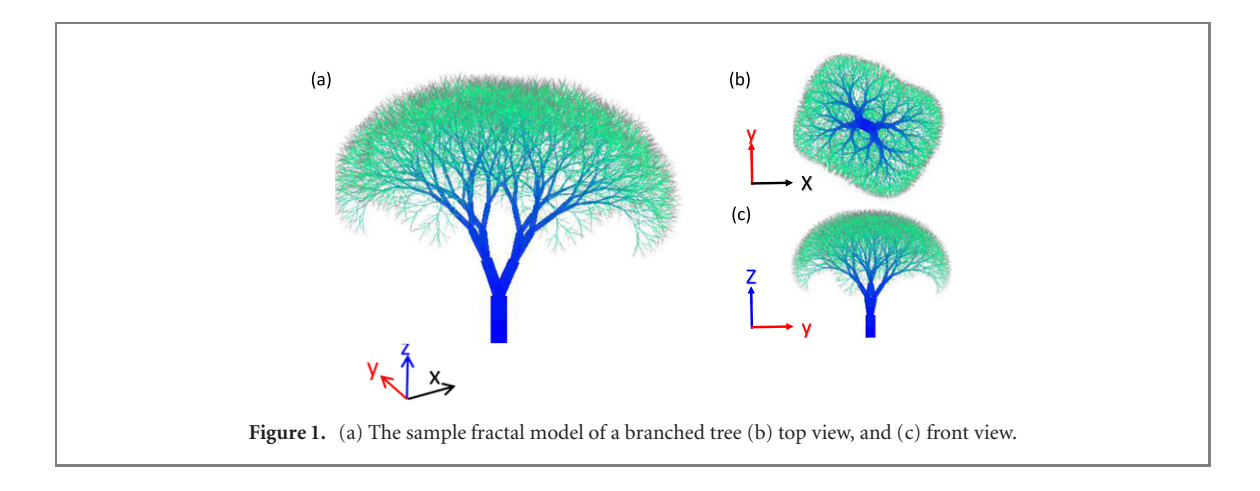
Wind-induced stress is the primary mechanical cause of tree failures. Among different factors, the branching mechanism plays a central role in the stress distribution and stability of trees in windstorms. A recent study showed that Leonardo da Vinci's original observation, stating that the total cross section of branches conserved across branching nodes is the optimal configuration for resisting wind-induced damage in rigid trees, is correct. However, the breaking risk and the optimal branching pattern of trees are also a function of their reconfiguration capabilities and the processes they employ to mitigate high wind-induced stress hotspots. In this study, using a numerical model of rigid and flexible branched trees, we explore the role of flexibility and branching patterns of trees in their reconfiguration and stress mitigation capabilities. We identify the robust optimal branching mechanism for an extensive range of tree flexibility. Our results show that the probability of a tree breaking at each branching level from the stem to terminal foliage strongly depends on the cross section changes in the branching nodes, the overall tree geometry, and the level of tree flexibility. Three response categories have been identified: the stress concentration in the main trunk, the uniform stress level through the tree's height, and substantial stress localization in the terminal branches. The reconfigurability of the tree determines the dominant response mode. The results suggest a very similar optimal branching law for both flexible and rigid trees wherein uniform stress distribution occurs throughout the tree's height. An exception is the very flexible branched plants in which the optimal branching pattern deviates from this prediction and is strongly affected by the reconfigurability of the tree.

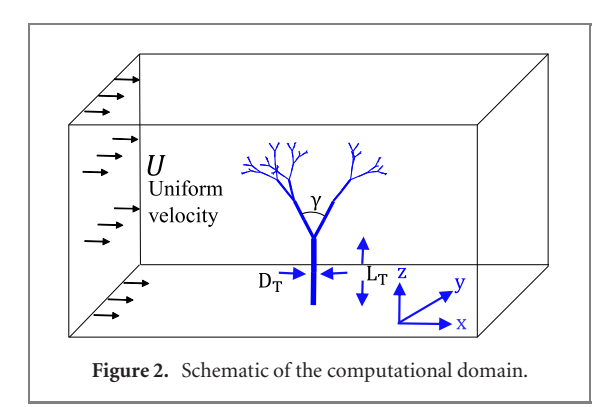
#### 1. Introduction

All plants need appropriate mechanical support to withstand dynamic and static environmental loads for their continual survival [1]. Plant movement can be classified as either spontaneous or as a result of a biological response to stimuli [2]. The latter will be the focus of this study. Trees and winds form a ubiquitous unit of the environment, in which the motion of trees affects and is affected by surrounding flow [3]. With the human effort to introduce trees in urban communities and the importance of such canopies for the ecosystem [4], it is crucial to assess the continual survival of trees in different environmental conditions.

The wind-induced motion of plants in normal wind conditions has various effects. It is used to

measure wind magnitude [5] and plays a vital role in dispersing seeds and pollen grains [6, 7]. The thermal [8, 9] gaseous exchanges along with transport [10, 11] of plants can also change when subjected to winds. The canopy height plays a central role in the light interception of plants [2, 12] whereby the fast movement of canopy top layers in the wind increases its light penetration and prompts an overall increase in the rate of photosynthetic induction [2]. Also, the oscillation of branches and leaves due to wind increases the carbon gain of canopies [13] and helps the water regulation of leaves with subsequent effects on the dynamics of pathogen development in the canopy [14, 15]. The motion of foliage in the wind also reduces arthropod herbivore infection [16, 17] and could be crucial for the plant's health. The damage to forests and crops from the turbulent





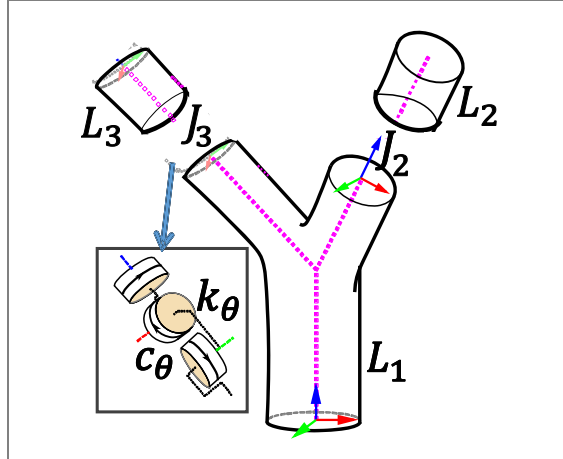


**Figure 3.** Tree branch connectivity.  $J_2$  and  $J_3$  are the joints connecting the mother branch-1 of length  $L_1$  to two daughter branches with lengths of  $L_2$  and  $L_3$  respectively. Here,  $k_\theta$  and  $c_\theta$  are the stiffness and damping of the joint, respectively.

flows during windstorms are another significant consequence of the interaction between wind and tree structures as they could cost billions of dollars to the US economy each year [18, 19].

There are four primary modes of tree damage due to wind-induced stresses: (1) base damage: occurs when the root of the tree breaks or there is soil instability beneath the tree; (2) trunk breakage: corresponds to the breakage of the tree stem; (3) branch breakage: occurs when any part of the upper elements of the tree breaks; and (4) excessive removal of the

leaves: is related to a chronic modification of the tree functionality [20, 21]. These damages occur because of rare high wind conditions; however, the tree posture can also change when exposed to strong winds for a long duration, tending to grow into a shape that results in uniform stress along the tree, among other factors. The growth pattern change in response to such winds is known as thigmomorphogenesis [22]. Mechanics of wind-induced stresses in trees have been extensively studied previously. Metzger [23] predicted that wind-induced stresses are constant along the length of tree branches and trunks. Mattheck [24] also recognized this hypothesis, suggesting that trees are optimized structures grown into perfect shape over time in which no part within the tree height is prone to more stress than other parts. However, recent studies have shown that wind-induced stresses vary by order of magnitude along the length of the tree. Niklas and Spatz [25, 26] disputed the constant stress hypothesis by calculating the wind-induced stresses of five Prunus serotina trees of the same species with different wind speed profiles and found that wind-induced stress varies along the length of the tree and depends on tree taper (geometry effect). Lopez et al [20] also showed that the location of the maximum stress in a fractal tree is dependent on its branching parameter. Lawton [27] predicted that an increase in trunk thickness helps withstand higher wind-induced stresses, and Milne and Blackburn [28] showed that the region associated with tree failure is the region of maximum stress. While the maximum stress level occurs in the trunk of some plant species, other species might experience high stresses at the top branches and foliage [20, 29]. In either case, breakage occurs at a point when the wind-induced stress exceeds the wood fracture strength [25].

Besides the uniform stress through the height, another strategy exists for trees to mitigate failure in high wind conditions. Tree species that lose their leaves and terminal branches/foliage are more likely to withstand severe hurricane storms [30, 31]. This is prevalent in larger trees because of their reduced flexibility and limited reconfiguration capabilities. This process is called wind-induced pruning [1], in

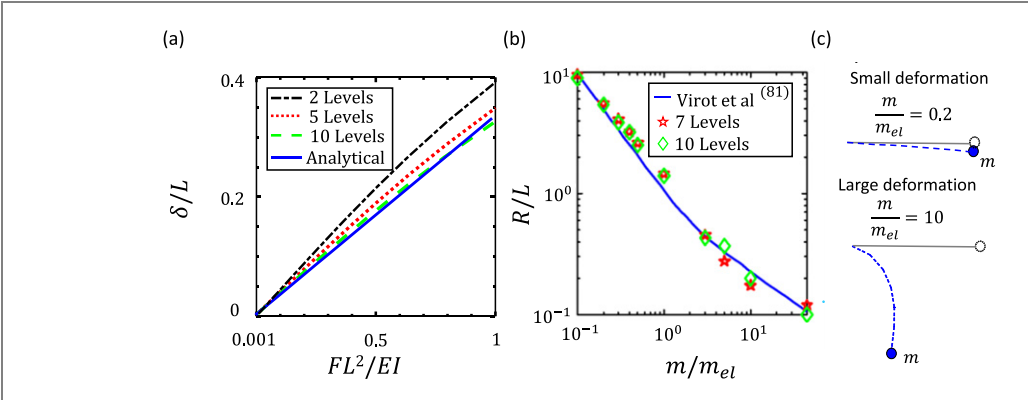


**Figure 4.** (a) Linear deformation of a beam as a function of the lateral force at the tip, (b) normalized radius of curvature as a function of normalized mass applied to the tip  $\left(\frac{m}{m_{\rm el}} = 0.1 - 40\right)$ , and (c) deflection patterns of the multi-link system with the attached mass of  $\frac{m}{m_{\rm el}} = 0.2$  and 10 with the seven-links model.

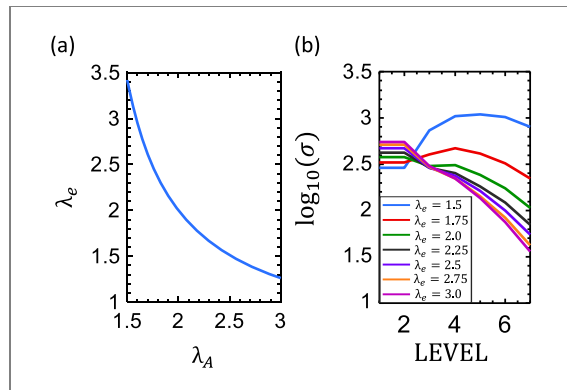


**Figure 5.** (a) Comparing the current branch ratio parameter,  $\lambda_{\rm A}$ , and the Hausdorff fractal parameter,  $\lambda_{\rm e}$ , used in Eloy [33], (b) total stress in different levels of the tree with  $\lambda_{\rm e}=1.5-3.0$ , and  $Ca=4\times10^{-5}$ .

which the wind loads acting on the tree reduce, and thereby, the tree maintains its upright stability.

Da Vinci, in his notebook, mentioned a general observation that 'all the branches of a tree at every stage of its height when put together are equal in thickness to the trunk (below them)' [32]. Da Vinci's observation that the summation of the surface area of all the daughter branches at every point of the tree equals the surface area of the mother branch was later linked with the most effective damage resistance in rigid branched trees [33]. Nonetheless, in reality, the rigid assumption of trees is a good approximation at low wind speeds. Almost all trees have a certain level of flexibility and undergo large deflection and reconfiguration in storm-wind conditions. They can reposition themselves with branches bending to reduce the wind forces and extend their survival range. Therefore, the stress level in the tree is also highly dependent on their capabilities in mitigating large wind forces and their ability to adopt a more aerodynamic shape and proper deflection [34, 35]. Tree branching has been studied over many decades, and although da Vinci's prediction is associated with uniform wind-induced stresses in rigid trees [33], other objectives have been proposed for fractal

shape trees with different branching mechanisms. For example, Murray, using the observed relation between branches' weight and circumference of nine trees, found that the branching ratio of mother (M) to daughter branches (Di) is 2.49 for large trees and 3 for small trees [36, 37] (e.g., the diameters satisfy  $D_M^{2.49} = D_{D1}^{2.49} + D_{D2}^{2.49}$ ). Zhi et al [38] found it to be 3 for small hairyleaf Japanese cherry trees and 2 for large ones. Minamino and Tateno [39] discussed that Fagus crenata and Abies homolepis trees (subjected to small wind forces) follow da Vinci's branching rule when the weight of the protruding lateral branch and the angle between branches are small, but the branching ratio decreases as these parameters increase. A similar repetitive branching structure is also observed in tree roots [40].

In this paper, we study how wind-induced stresses in trees are affected by tree flexibility, in addition to geometry effects, and examine if there is a particular branching sequence that results in uniform stress distribution in moderately flexible trees. It is motivated by observing that when plants are flexible, they can reconfigure and experience lower drag [41]. Two main analytical models previously proposed to study wind stress in trees are a discrete self-similar branch structure through the tree [33] and the continuous tapered beam model [42]—an unbranched beam with underlying dynamics similar to a branched beam. Lopez et al [29], using a bundle of tapered beams, found that the flow-induced drag reduction of trees during reconfiguration either by bending [43–46], pruning [20], or a combination of both is comparable and such changes in the shape ensure survival under harsh winds. On the other hand, a self-similar fractal model of the trees has only been applied to the rigid trees, and it is still unknown what the combined role of reconfiguration and branching architecture is for excurrent and decurrent tree species [47-49]; and whether the previous predictions about the optimal design of branched rigid trees [33] applies to reconfigurable systems. We will later show that there is a particular branching mechanism

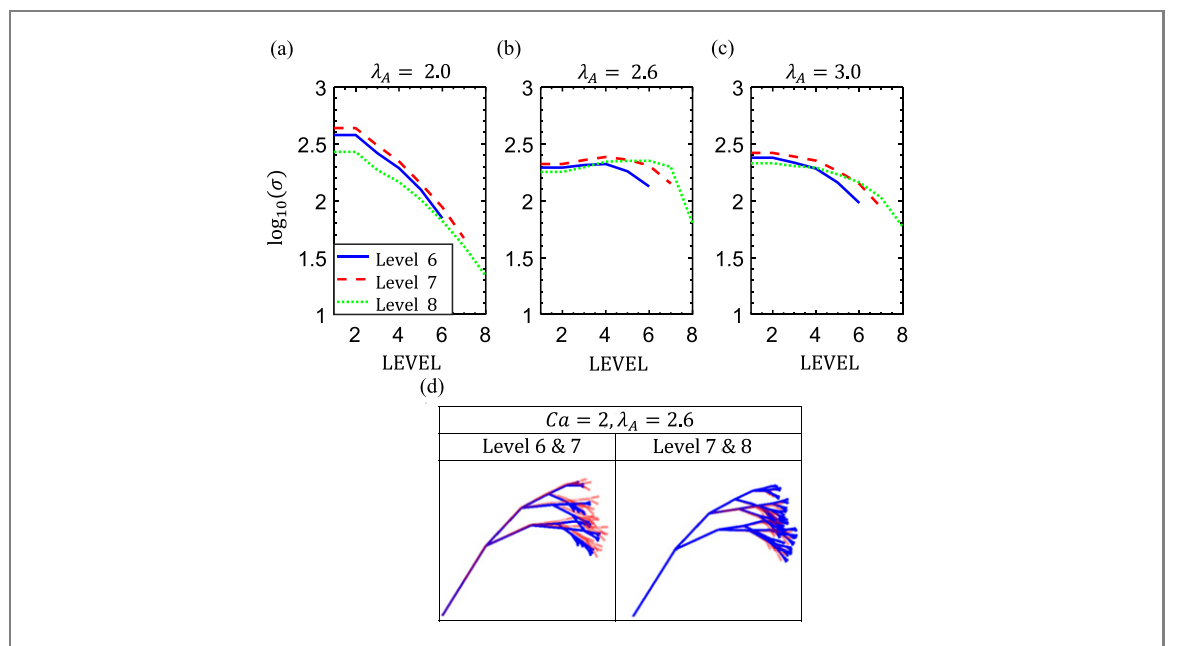


**Figure 6.** (a)–(c) Comparison of stress distribution in a tree with six, seven, and eight branching levels for  $\lambda_A = 2.0$  (a), 2.6 (b), 3.0(c). (d) Deflected shape of the tree with six and seven branching levels (left), seven and eight branching levels (right). The base case of seven branching levels is shown with the red color.

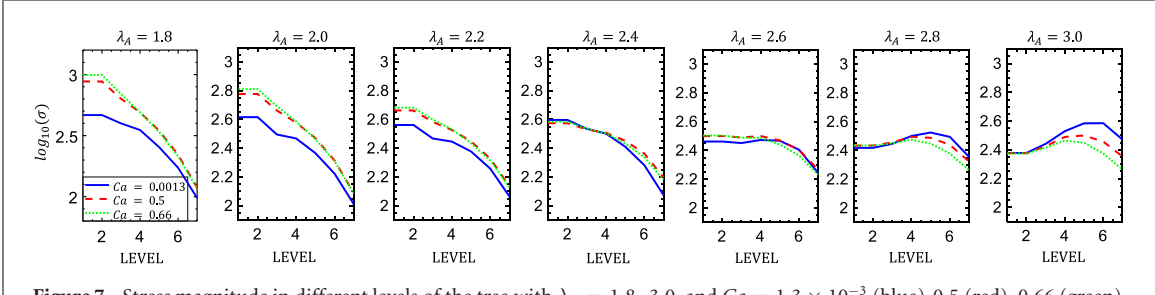


Figure 7. Stress magnitude in different levels of the tree with  $\lambda_A = 1.8-3.0$ , and  $Ca = 1.3 \times 10^{-3}$  (blue), 0.5 (red), 0.66 (green).

that promotes uniform stress at all levels across a wide range of moderately flexible trees.

Three methods can be employed to solve the dynamic response of tree structures relevant to this study: (1) lumped-mass method: in this technique, the branch mass is concentrated at a discrete point (top of the branch) as it deforms [34, 50-53]; (2) generalized displacement method: this method assumes a uniformly distributed mass for each branch along its length [21, 54-56]; and (3) finite element method (FEM): FEM is the generalization of both lumped-mass and generalized displacements methods [57-60]. It divides a branch into an appropriate number of elements, with each element becoming the generalized coordinate. A tree is an inhomogeneous structure, and its properties, such as its branch stiffness and branching shapes, are mostly anisotropic and change across species. All these conditions have to be considered in the model for a more accurate representation, which is only possible with the FEM method. FEM, however, is an expensive computational model for branched trees and requires accurate measurements of many parameters and loading conditions to reach accurate results [61]. This is a

significant challenge in using FEM for a comprehensive study of tree branching effects and identifying characteristic parameters that can quantify the reconfiguration capabilities of the system. Therefore, certain simplifications should be made given the variety of shapes and parameters that trees can attain. This paper follows the previous works [33, 62, 63] and assumes that the tree structure follows a fractal law. Moreover, we model each tree branch as a rigid link connected to neighboring branches at its end joints to reach a simple representative model. This assumption is consistent with previous research on dynamic tree models [52, 53, 60]. We also neglect the dynamic effect of leaves on the tree dynamics, assuming the tree has a uniform number of branches in its crown, and each branch is exposed to a constant uniform wind speed without temporal changes. Moreover, it is assumed that the lift and drag coefficients are similar across different branches to efficiently identify the role of flexibility on the branching mechanism's scaling

The rest of the paper is organized as follows: section 2 describes the problem description. Section 3 contains detailed descriptions of the mathematical model and its validation, followed by results and discussions in section 4. Finally, the conclusion, along with a discussion about the importance and significance of our findings, is presented in section 5.

### 2. Problem description

#### 2.1. Problem setup

The branched tree in this study is modelled as a self-similar fractal structure [33, 53, 64] in which each leading mother branch (at level k) connects to two succeeding daughter branches (at level k+1). The same branching mechanism is repeated at every joint, resulting in  $N_q$  total joints. A sample generated model tree is shown in figure 1. To reach a tractable computational model of the branched tree dynamics, it is assumed that all the branches are rigid and connect to their parents and daughters with rotational joints, each joint with two degrees of freedom (DOF) in bending, as shown later in the paper in figure 3. This assumption considerably reduces the size of the original problem to  $2N_q$  equations for the angular

rotation  $(\mathbf{q}_{2N_q})$  of  $N_q$  joints. The gravity and wind forces acting on branches (hereafter are referred to as links) are transferred to joints, and depending on the joints' stiffness, they lead to geometrical changes in the tree. The torsional and axial deformations are not considered as their effects on the tree reconfiguration are found to be secondary compared to the bending deflection of the branches. The tree is connected to the ground through a joint with stiffness associated with the trunk length and diameter. It is assumed that the steady wind acts along the x-axis on each tree branch. The schematic setup of the tree is shown in figure 2.

The tree geometry is constructed such that the junctional change in cross sectional areas (parametrized with  $\lambda_{\rm A}$ ) and the branches' length (parametrized with  $\lambda_{\rm I}$ ) are constant through the tree height, making the tree self-similar, as shown in figure 2. The flexibility of the tree structure is characterized by two parameters: the slenderness ratio  $(D_{\rm T}/L_{\rm T})$ , defined as the ratio of the trunk diameter to its height, and the bending flexibility of the trunk. The nondimensional parameters used in the simulation are

$$\lambda_{A} = \frac{A_{k}}{A_{k+1}} = \left(\frac{D_{k}}{D_{k+1}}\right)^{2}, \quad \lambda_{L} = \frac{L_{k}}{L_{k+1}}, \quad Ca = \frac{\rho_{\text{air}}U^{2}L_{\text{T}}^{4}}{2EI}, \quad Fr = \frac{U}{\sqrt{gL_{\text{T}}}}, \quad M^{*} = \frac{\rho_{\text{wood}}}{\rho_{\text{air}}}.$$
 (1)

Here  $A_k$ ,  $D_k$ , and  $L_k$  are the cross sectional area, diameter, and length of a mother branch of the joint  $k \to k+1$ , while  $A_{k+1}$ ,  $D_{k+1}$ , and  $L_{k+1}$  are the corresponding quantities for one of the identical daughter branches.  $\rho_{\rm air}$  is the density of air,  $\rho_{\rm wood}$  is the tree density, here its chosen to be similar to an oak tree species. We also assume uniform wind velocity U on every branch, chosen to be in the order of a category three hurricane, and  $L_T$  is the length of the trunk. Cais the Cauchy number comparing the dynamic flow force to the rotational stiffness (EI) of the trunk. The Froude number, Fr, represents the nondimensional gravity (g) effect. Other parameters which define the mechanical status of a branched tree are the branching number,  $n_b$ , defined as the number of daughter branches that originate from a mother branch at each junction and the separation angle between daughter branches ( $\gamma$ ). Here, we follow the previous setup by Eloy [33] and choose  $n_b = 2$ . In addition, it is assumed that  $M^* = 600$  and we investigate the effects of Ca and  $\lambda_A$  on the plant reconfiguration and wind load tolerance. The effect of  $D_{\rm T}/L_{\rm T}$ , Fr,  $\gamma$ and  $\lambda_L$  on the observed trends are then discussed subsequently. The range of geometrical parameters considered here are consistent with what is observed in naturally occurring trees. For example, the  $\lambda_A$ range covers hairy Japanese cherry, oak, A. homolepis,

bitternut, *F. crenata* [36, 38, 39] and  $\lambda_L$  range covers *Salicornia europaea*, fir, and pine [65, 66]. Table 1 summarizes the parameters considered in this study. Unless otherwise mentioned, the simulation results are for Fr = 11.3,  $\lambda_L = 0.7$ ,  $\gamma = 45^\circ$  and  $D_T/L_T = 0.3$ . The sensitivity of the results to the variation of each selected parameter is discussed in appendix A.

#### 2.2. Multi-link model of a branched tree

An interconnecting multi-link model of a branched tree is used here, wherein each link is connected to its precedent mother link with two rotational DOF at the interconnecting joint, as depicted in figure 3. The first branch with length  $(L_1)$  is connected to a small segment with infinitesimal length attached to the ground (the base branch-0) with joint  $(J_1)$ , and then connected to its two succeeding branches with lengths of  $L_2$  and  $L_3$  at the joints  $J_2$  and  $J_3$ . Each interconnected joint has the same EI, and its rotational stiffness is calculated from  $k_{\theta} = \frac{2EI}{\rho_{\text{air}}U^2L_{\text{T}}^4\lambda_{\text{A}}^{2(k-1)}(L_T/L_k)}$ , following the scaling law of a cantilever beam with a unit moment at its tip. The joints are assumed to be viscoelastic with the damping of  $c_{\theta}$ . The same geometrical progression continues at other levels in the tree (figure 2). The tree's topology is represented with a connectivity vector (*C*), which identifies the parent

Table 1. Characteristic parameters and their ranges.

Parameter	Range
Ca	$6.7 \times 10^{-5}$ – $10$
$\lambda_{A}$	1.8-3.0
$M^*$	600
Fr	1–30
$D_{ m T}/L_{ m T}$	0.1-0.8
$D_{\mathrm{T}}/L_{\mathrm{T}}$ $\lambda_{\mathrm{L}}$	0.4-1.0
$\gamma$	$45{ ext{}}105^{\circ}$

sequence of each link. The number of connections in the tree per level varies by a factor of two, resulting in  $2^{k+1}$  connections from the stem to the branching level.

# 3. Methodology

#### 3.1. Mathematical model of the tree structure

The translational and rotational dynamics of the tree are modeled using the Newton–Euler equations [67–69] of rigid links. The equation of motion of each link, for instance, Link-*k*, can be written as

$$f_k = m_k \dot{v}_k, \tag{2}$$

$$T_k = \mathbf{I}_k \dot{\boldsymbol{\omega}}_k + \boldsymbol{\omega}_k \times (\mathbf{I}_k \boldsymbol{\omega}_k), \tag{3}$$

where  $f_k$  is the resultant force vector (includes external loads and the forces exerted on the link by its attached joints) acting on link k,  $m_k$  is the mass, and  $v_k$  is the linear velocity vector at the center of mass (CoM) of link k.  $T_k$  is the resultant torque acting on the CoM, while  $I_k$  and  $\omega_k$  are the rotational inertia matrix and angular velocity of the kth link, respectively.

Equations (2) and (3) can be combined and expressed as

$$\mathbf{f}_{k}^{o} = \mathbf{M}_{k} \dot{\varepsilon}_{k} + \mathbf{f}_{k}^{n}, \tag{4}$$

where the combined force  $f_k^o = [f_k^T, T_k^T]^T$  is the summation of the external  $(f_k^e)$  and the interaction combined forces from the link-link coupling at the joints of link k  $(f_k^i)$ ,  $\mathbf{M}_k = \mathrm{diag}(m_k \mathbf{I}_{3\times 3}, \mathbf{I}_k)$ ,  $\varepsilon_k = [\boldsymbol{v}_k^T, \boldsymbol{\omega}_k^T]^T$  and  $f_k^n = [\mathbf{0}_{1\times 3}, (\boldsymbol{\omega}_k \times \mathbf{I}_k \boldsymbol{\omega}_k)^T]^T$ . The combined velocity vector,  $\varepsilon_k$ , is a combination of the angular velocity  $\boldsymbol{\omega}_k$  and the linear velocity  $\boldsymbol{v}_k$  of link k and is calculated using the forward recursion technique from the fixed base [70]. The position of the deformed tree, or equivalently the joints rotations,  $\boldsymbol{q}_k$ , are iteratively calculated from the joint angles of preceding links. In particular, the velocity of the branch k can be related to joints' rotation with,

$$\varepsilon_{k} = \begin{bmatrix} \mathbf{J}_{v,k}(\boldsymbol{q}) \\ \mathbf{J}_{\omega,k}(\boldsymbol{q}) \end{bmatrix} \dot{\boldsymbol{q}} = \mathbf{J}_{c,k}(\boldsymbol{q}) \dot{\boldsymbol{q}}, \tag{5}$$

where  $\mathbf{J}_{c,k}(\mathbf{q})$  is a 6 × 2 $N_q$  matrix whose elements are, in general, nonlinear functions of joint angles. It is

called the Jacobian matrix of the algebraic system and is expressed in the same coordinate frame as the spatial velocity  $\varepsilon_k$ . Here,  $\mathbf{q} = [q_1, \ldots, q_k, \ldots, q_{2N_q}]^T$  is the vector of joints' rotations chosen as the generalized coordinates of the tree structure and  $\dot{\mathbf{q}}$  is its time derivative. The connectivity vector is utilized to calculate the non-zero components of  $\mathbf{J}_{c,k}$  efficiently, and to determine which joints alter the motion of a particular link. If there is no such connection, the corresponding column of  $\mathbf{J}_{c,k}$  is set to zero. The velocity and acceleration of all branches can be written similarly as,

$$\varepsilon = \mathbf{J}_{c}\dot{\boldsymbol{q}},\tag{6}$$

$$\dot{\varepsilon} = \mathbf{J}_c \ddot{\mathbf{q}} + \dot{\mathbf{J}}_c \dot{\mathbf{q}},\tag{7}$$

and equation (4) can be written as

$$f^{o} = \mathbf{M}(\mathbf{J}_{c}\ddot{\boldsymbol{q}} + \dot{\boldsymbol{J}}_{c}\dot{\boldsymbol{q}}) + f^{n}, \tag{8}$$

$$f^o = \mathbf{MJ}_c \ddot{q} + f^c, \tag{9}$$

where  $f^c = \mathbf{M}\dot{J}_c\dot{q} + f^n$  is the summation of all velocity-dependent inertial forces and torques acting on the centers of mass of the branches. Furthermore, by multiplying by  $\mathbf{J}_c^T$ , we obtain

$$\mathbf{J}_{c}^{T} \mathbf{f}^{o} = \mathbf{J}_{c}^{T} \mathbf{M} \mathbf{J}_{c} \ddot{\mathbf{q}} + \mathbf{J}_{c}^{T} \mathbf{f}^{c}, \tag{10}$$

and with the definition of  $\mathbf{J}_c^T f^e = \boldsymbol{\tau}^e$ ,  $\mathbf{J}_c^T f^i = \boldsymbol{\tau}$ ,  $\mathbf{J}_c^T \mathbf{M} \mathbf{J}_c = \mathbf{H}$ , and  $\mathbf{J}_c^T f^c = \boldsymbol{c}$ , equation (10) can be compactly rewritten as

$$\mathbf{H}\ddot{\mathbf{q}} + \mathbf{c} = \mathbf{\tau}^{\mathrm{e}} + \mathbf{\tau},\tag{11}$$

where  $\tau^e$  is the generalized external forces and torques associated with the generalized coordinate system q. In addition, the reaction forces from the joints [68],  $\tau = [\tau_1, \ldots, \tau_k, \ldots, \tau_{2N_q}]^T$ , is defined as  $\tau_k = k_{\theta,k}q_k + c_{\theta,k}\dot{q}_k$  to model the reactive force from the flexibility of the joint k. Here,  $c_{\theta,k}$  is the stiffness proportional damping defined as  $c_{\theta,k} = 0.1k_{\theta,k}$  [47, 64]. However, the final steady-state reconfiguration shape of the branches is independent of this parameter. Renaming  $\tau^e + \tau = \Gamma$ , equation (11) is recast into a generalized space-state form with the definition of the angular velocity of joints  $p = \dot{q}$ ,

$$\begin{bmatrix} \Gamma \\ p \end{bmatrix} - \begin{bmatrix} \mathbf{H}(p,q) & \mathbf{0} \\ \mathbf{0} & \mathbf{I} \end{bmatrix} \begin{pmatrix} \dot{p} \\ \dot{q} \end{pmatrix} = \begin{pmatrix} c \\ \mathbf{0} \end{pmatrix},$$

and is discretized with the implicit Euler method as

$$\begin{bmatrix} \mathbf{\Gamma}^{n+1} \\ \mathbf{p}^{n+1} \end{bmatrix} - \Delta t^{-1} \begin{bmatrix} \mathbf{H}(\mathbf{p}^{n+1}, \mathbf{q}^{n+1}) & \mathbf{0} \\ \mathbf{0} & \mathbf{I} \end{bmatrix} \begin{pmatrix} \mathbf{p}^{n+1} - \mathbf{p}^{n} \\ \mathbf{q}^{n+1} - \mathbf{q}^{n} \end{pmatrix} = (\mathbf{c}^{n+1}\mathbf{0}).$$
(12)

The resulting fully nonlinear equation is solved with an inexact matrix-free Newton–Krylov technique, using an inexact Newton backtracking outer nonlinear solver, along with the GMRES inner linear solver [71, 72]. The convergence tolerance and the maximum number of iterations are  $10^{-7}$  and 100 respectively. Both constants were sufficient for the convergence of the current system with multiple temporal and spatial scales.

#### 3.2. Wind and gravity forces

Two types of external forces act on the tree, namely, the downward gravity force  $(F_{\rm g})$  and wind-induced drag force  $(F_{\rm w})$ , each scaling differently with the branch sizes,  $|F_{\rm g}| \propto D^2 L$  and  $|F_{\rm w}| \propto DL$  where D and L are typical branch diameter and length, respectively. The effect of gravitational forces is important for moderately flexible and flexible trees where significant bending deformation occurs [73-76] (section 4.4). Without the wind action, the weight of branches causes a prestressed configuration [1]. The combined forces acting on each link are transferred to its nearest joints which change the angles of these joints. The process of combining these forces starts from the topmost branches and continues to the trunk.

The aerodynamic drag force acting on a link per unit length has two components: (1) normal to the branch  $(f_n)$  and (2) tangential to the branch  $(f_t)$  according to

$$f_{\rm n} = \frac{1}{2} \rho_{\rm air} C_{\rm n} |V| [V - (V \cdot t)t] D,$$

$$f_{t} = \frac{1}{2} \rho_{air} C_{t} |V| (V \cdot t) t \pi D, \qquad (13)$$

where D is the diameter of the branch.  $C_n$  and  $C_t$ are normal and tangential drag coefficients of each link, respectively, t is the tangential direction, and V is the apparent wind velocity approaching the considered branch segment. The exact values of  $C_n$  and  $C_{\rm t}$  depend on the surface roughness and orientation of the branches and is modified with their flowinduced motion and aerodynamic interaction with each other. Here, we simplify the problem and instead use  $C_{\rm n} = 1$  and  $C_{\rm t} = 0.1$  for a circular cross-section. The actual value of  $C_t$  (skin-friction drag) of a smooth cylinder can be calculated from the shear frictional stress on the surface of the cylinder, and with a specific boundary layer approximation, can be related to the orientation of the branch and approaching Reynolds number [77, 78]. Overall, we observed that the system's response, as discussed in appendix B, does not substantially change with the modification

of drag coefficients. It is also assumed that the aerodynamic force from the truncated portion of the tree can be represented with  $C_{\rm n}=1$  for a disk with a radius of the terminal branch. This contribution is imposed at the tip of terminal branches.

The total force and torque on each branch are calculated from the line integration of  $f_n$  and  $f_t$ . The joint forces, along with the nonlinear inertial forces, c in equation (11), are transmitted from the top links of the tree to the first link (trunk) using the backward recursion technique [70]. An entire loop of the forward and backward recursions is employed for the concurrent calculation of total linear forces and moment acting on the joints and efficient setup of the inertial matrix of the multi-link system, H (equation (11)).

#### 3.3. Model validation

Linear and nonlinear validation tests were done to verify the accuracy of the tree model. The linear validation is based on the calculation of the deflection in an unbranched tree and comparing it with the analytical deflection of a beam solution  $\left(\delta = \frac{FL^3}{3EI}\right)$ . F is the applied transverse force, E is Young's modulus of the tree, I is the moment of inertia of the circular tree, and L is the total length of the beam. Trees with two, five and ten unbranched tree levels were considered here. A stiffness constant  $k_{\theta} = \frac{EI}{L_{\nu}}$ [79, 80] is used for all the links, where  $L_k$  is the length each link. Figure 4(a) shows the comparison between the deflection results from the simulation and the analytical method. It is observed that by increasing the number of links, the numerical results approach the analytical results. Overall, the results verify the accuracy of the multi-link model used in this study.

As a second validation case for larger deflection scenarios, the mass (m) is attached to the last link of a horizontal beam as shown in figure 4(b), and its magnitude increases gradually to test the model for small (linear) to large (nonlinear) deformation ranges, according to Virot et al [81]. The normalized mass is  $m/m_{\rm el}$  where  $m_{\rm el}$  is characteristic mass defined as  $m_{\rm el} = EI/gL^2$ . We compare R/L, the normalized radius of maximum curvature along the length. When a small attached mass is applied, the multi-link beam is weakly bent  $(R/L \gg 1)$ , but with the increase of the attached mass, it shows large deformation and localized small radius of curvature  $(R/L \ll 1)$ . Figure 4(b) shows that R/L, scales with  $(m/m_{\rm el})^{-1}$ when the deformation is small and  $\left(m/m_{\rm el}\right)^{-1/2}$ at large deformations when  $\frac{m}{m_{\rm el}} = 0.1$ –40 while the beam deflection patterns for  $\frac{m}{m_{\rm el}} = 0.2$ , and 10 are shown in figure 4(c). The simulation results with seven and ten levels show a good match with the experimental results by Virot et al [81]. Each tree branch is modeled as a single link to form a simple but representative model of dynamic fractal trees. However, the sensitivity of the overall tree deflection and

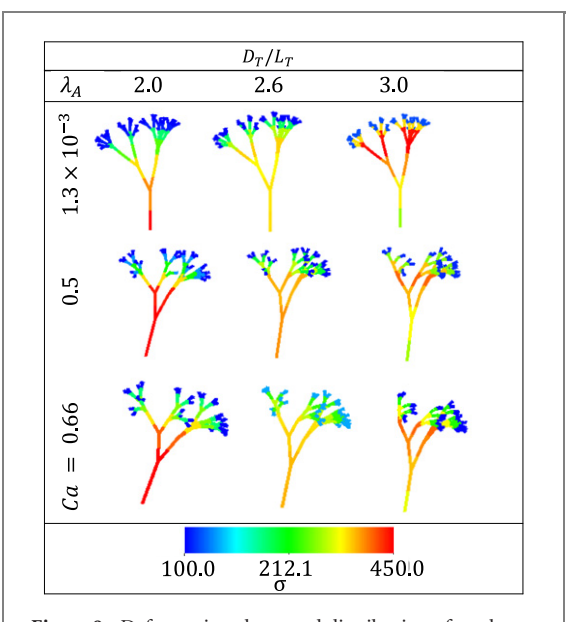


**Figure 8.** Deformation shape and distribution of total stress in the branches for  $Ca = 1, 3 \times 10^{-3}, 0.5, 0.66$  and  $\lambda_A = 2.0, 2.6$ , and 3.0.

stress profile based on this assumption is discussed in appendix C.

Also, we validated our model with the fractal diameter relation used previously by Eloy [33]:  $\frac{D_k}{D_{k+1}} = n_b^{\frac{1}{\lambda_e}}$ , from the stem to the top branch where  $n_{\rm b}$  is the number of protruding daughter branches at each joint (it is two here), and  $\lambda_e$  is the fractal (Hausdorff) dimension of the thickness of the tree skeleton. Equating the diameter relation of our model (section 2.1) with that of Eloy and comparing the branching ratios ( $\lambda_A$ ,  $\lambda_e$ ) as seen in figure 5(a), we found that they are inversely proportional, with an exponential decay of  $\lambda_e$  occurring when  $\lambda$  increases. Also, in our simulation for a rigid tree case (approximated as a very stiff tree with  $Ca = 4 \times 10^{-5}$ ), it was found that the total stress ( $\sigma$ ) experienced by the tree is more uniform at  $\lambda_e = 2$ . At lower  $\lambda_e$  values, the tree experiences maximum stress at the top branch while at higher  $\lambda_e$  values, the highest stress appears at the tree's trunk, as shown in figure 5(b). This result is consistent with the previous prediction by Eloy [33] that  $\lambda_e = 2$  results in uniform stress and offers the best resistance to wind-induced fracture in fractal rigid trees.

#### 3.4. Model setup

In figures 6(a)-(c), we compare the average nondimensional stress versus the branching level of three model trees with the truncation level of six, seven and eight. The average stress is computed from the ensemble averaging of branches at a particular branching level and three  $\lambda_A$  values of 2.2, 2.6, 3.0. Other parameters are fixed at their characteristic values given in section 2.1. While the stress distribution along a tree modifies with more levels, the stress variations with seven and eight levels are very similar. It is found

that the forces exerted on small terminal branches in levels larger than seven do not change the deflected shape of the trees, as can be seen in figure 6(d). This suggests that seven levels of branching are sufficient to capture all the dominant wind-induced dynamics of a tree model, and the inclusion of smaller branches at higher levels only marginally alters the results, including the maximum stress distribution. Our tree model is then truncated at the seventh level to limit the computational expenses.

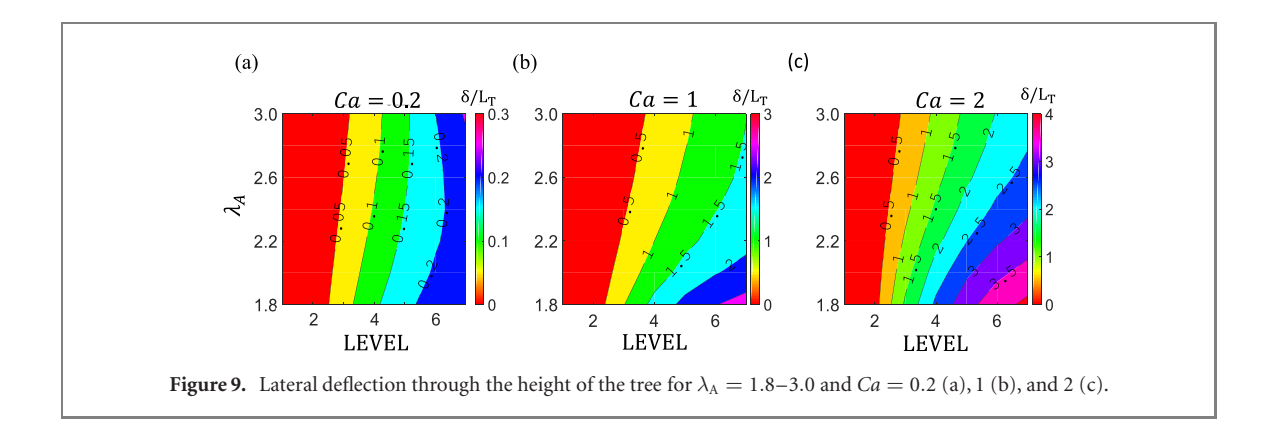
Seven initial random realizations of each setup are tested to account for the random orientations of the tree and the incoming wind, and the average stress values of the group are reported. This number of realizations is found sufficient in capturing the mean statistics. Each simulation is started with no wind and gravity forces. Gravity is first introduced over  $20\ L_T/U$ , and then the wind and gravity gradually increase to their nominal values. The results are calculated when the transient responses pass and the tree reaches its equilibrium configuration.

#### 4. Results

There are two types of forces that contribute to the total stress in the tree: (1) gravity and (2) aerodynamic forces [73, 75, 82]. Wind-induced stress from the aerodynamic force is the more critical component in predicting the structural stability of trees in storms. When trees grow, their growth rate reduces, causing the primary branches to thicken and smaller branches to become curved to minimize the gravity effect [60, 83, 84]. However, gravitational-induced loads, which are almost negligible for stiff trees, could induce a considerable increase in stress for more flexible branches when they are subjected to high wind speeds [73, 74] (section 4.4). Since the focus of this study is to explore how the tree reconfiguration affects the stress distribution, we do not differentiate between the gravity and wind forces, and both environmental forces are considered simultaneously.

#### 4.1. Effect of branching ratio $\lambda_A$

Three different flexibility levels are considered here with  $Ca = 1.3 \times 10^{-3}$  (stiff tree), 0.5, and 0.66 (moderately flexible). At a lower branching ratio ( $\lambda_A = 1.8-2.2$ ), the tree experiences a steep reduction of  $\sigma$  from the trunk (level 1) to the top branch (level 7), as shown in figure 7. This is associated with a reduction in the cross section with the branching level. An overstress hotspot, i.e., an isolated location with maximum stress is consistently found at level 1. As Ca increases, the tree becomes more flexible, and similar stress distribution is observed. This suggests that the flexibility has a secondary effect on the stress distribution in the tree compared to the branching ratio. The maximum stress, however, constantly increases at the trunk with an increase in Ca. The change is



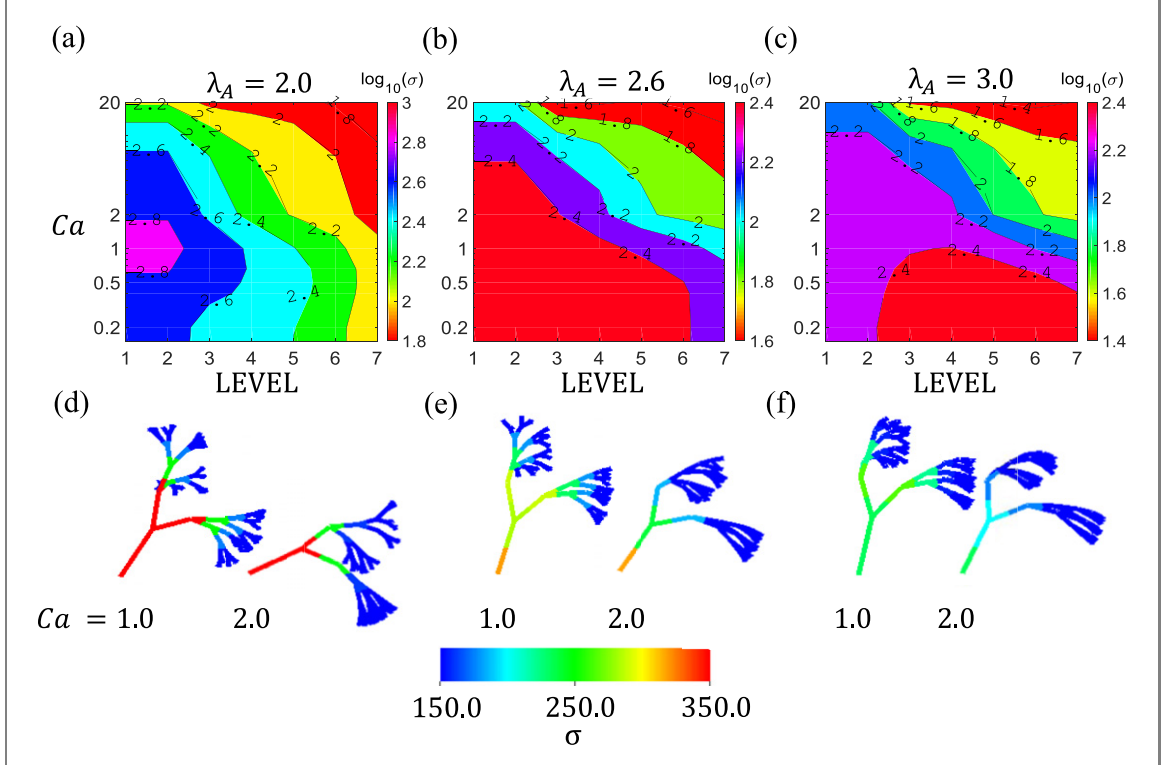


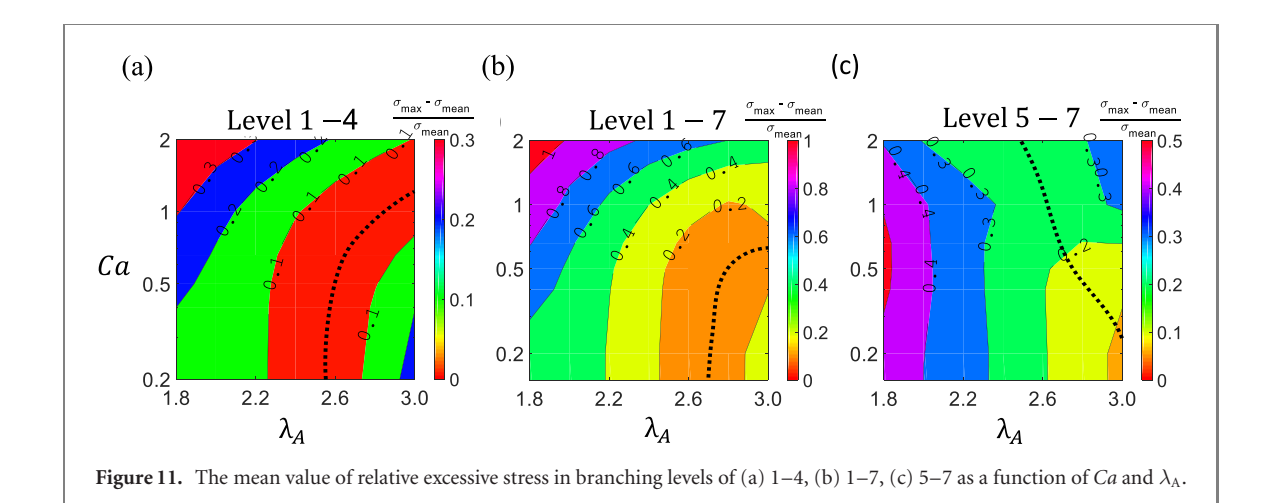
**Figure 10.** (a)–(c) Stress magnitude through the height of the tree as a function of Ca, when  $\lambda_A = 2.0$  (a), 2.6 (b), 3.0 (c), (b)–(f) the stress distribution and tree deflection for Ca = 1.0, 2.0 at  $\lambda_A = 2.0$  (d), 2.6 (e) and 3.0 (f).

attributed to competing effects of wind and gravity in the deformable branches.

Based on our previous definition of  $\lambda_A$ , an increase in  $\lambda_A$  means each protruding branch has a smaller cross section as the tree level increases, according to  $D_{k+1} = \frac{D_k}{\sqrt{\lambda_A}}$ . Therefore, as the branching ratio increases ( $\lambda_A = 2.4 - 2.6$ ), top branches have a smaller diameter and undergo more significant reconfiguration to keep the  $\sigma$  almost constant for all Ca. For higher  $\lambda_A$ ,  $\lambda_A = 2.8 - 3.0$ , the position of maximum  $\sigma$  shift toward the top branches. This is due to the large deformation of the more slender top branches and the contribution of their weights. In these cases, the trees' failure mode is shifted to higher branches. As shown in figure 7,  $\lambda_A = 2.6$  is the optimal branching ratio because it yields the most uniform stress through the tree height. The optimal branching parameter is consistent with previously observed values in trees

[36, 38], suggesting that the branching pattern is not significantly modified with variations in the wind speed and other initial conditions.

From the results, we can say that three survival mechanisms might be adopted in different tree species based on the branching mechanism, here  $\lambda_{\rm A}$ . For a small branching ratio, the tree requires stronger material near its base and a robust anchoring mechanism near to the ground to survive harsh wind conditions. For a moderate  $\lambda_{\rm A}$  range, the tree leverages its well-balanced geometrical characteristics to redistribute environmental forces through its height optimally and, therefore, eliminates the localized stress hotspots. In this case, the whole structure contributes to the survival envelope through reconfiguration, and if the tree eventually undergoes failure, it could break at any random position in its height. For larger  $\lambda_{\rm A}$  or equivalently faster tapering towards the top



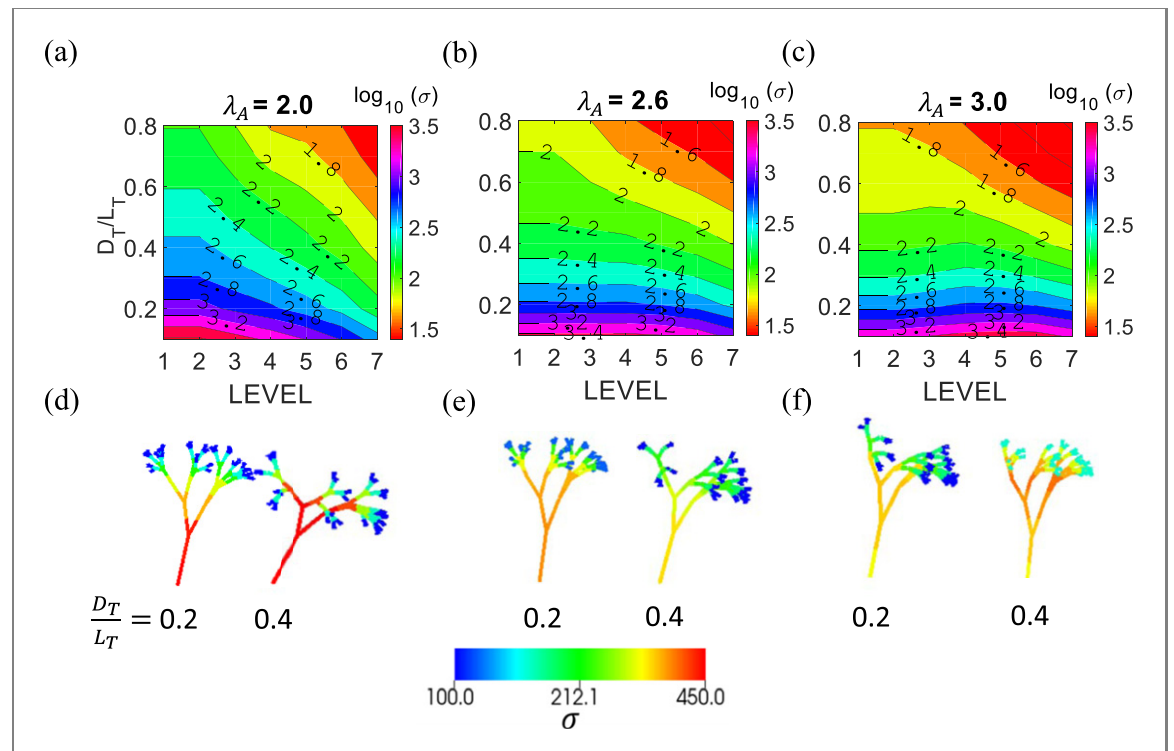


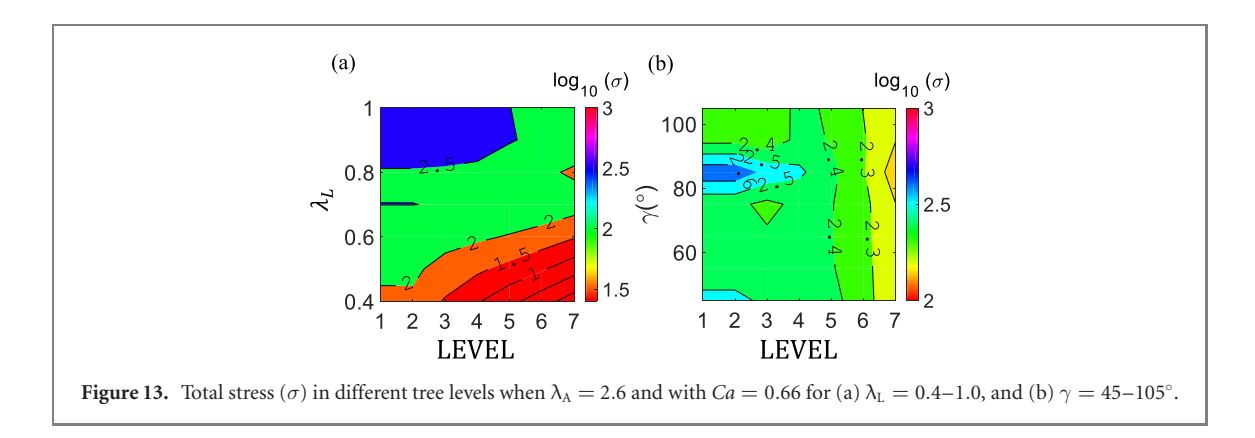
**Figure 12.** (a)–(c) Changes of stress magnitude ( $\sigma$ ) through the tree's height for  $D_{\rm T}/L_{\rm T}=0.1$ –0.8 and  $\lambda_{\rm A}=2.0$  (a), 2.6 (b), 3.0(c). (d)–(f) Deflection shape and stress distribution for  $\lambda_{\rm A}=2.0$  (d), 2.6 (e) and 3.0 (f). Here, we assumed a fixed Ca=0.66.

branches, most deformation and stress concentration is located at the top levels due to large deflection and secondary gravity actions. Such tree shapes might be an alternative natural survival mechanism where the potential breakage is encoded in the terminal branches to effectively reduce the wind actions on the rest of the tree.

For further analysis of the stress state, three distinct stress distributions with  $\lambda_A = 2.0, 2.6, 3.0$ , are selected. The deformation pattern of the tree can be seen in figure 8. More localized reconfiguration states are associated with larger Ca and larger  $\lambda_A$ . These two factors are found to play complementary roles in regulating the deflection mode of the tree. It is found that although the tree flexibility induces an asymmetric shape with a potential increase in gravity-

induced stress, the overall stress still decreases due to the reconfigurability of flexible trees.

To further explain how the deformation pattern of a tree changes with tree branching, the Euclidean distance  $(\delta/L_T)$  of the CoM of all the members of each branching level in the deformed tree from the corresponding point in the undeformed tree is shown in figure 9. For stiff trees (Ca=0.2) shown in figure 9(a), the tree experiences an approximately linear increase in deformation at each tree level. A different trend is seen for more flexible cases. For  $Ca \ge 1$  (figures 9(b) and (c)), we observe that the rapid increase in branch deformation depends on the branching level and Ca. For example, at  $\lambda_A = 3.0$  and Ca = 2, deformation increases rapidly at levels  $\ge 2$ , while it occurs for levels  $\ge 4$  for Ca = 1. Persistently,



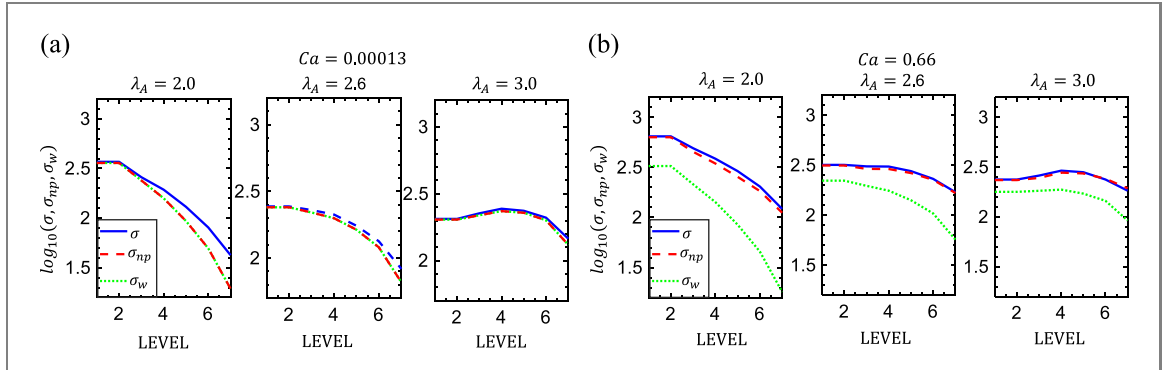
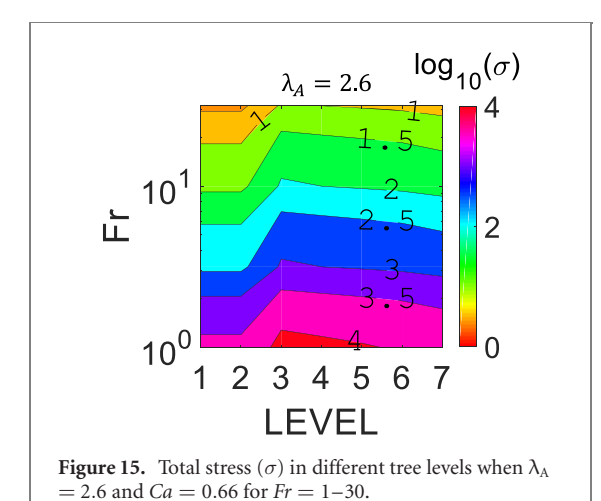


**Figure 14.** Total stress, total stress without static loads, and wind-induced stress  $(\sigma, \sigma_{\rm np}, \sigma_{\rm w})$  across tree levels. Subplots (a) are for a stiff tree with  $Ca = 1.3 \times 10^{-4}$ , and subplots (b) are for a flexible tree with Ca = 0.66.



the deflection pattern becomes local with an increase of  $\lambda_A$  while the deflection magnitude is similarly affected by Ca for all branching ratios.

#### 4.2. Effect of Cauchy number

Different Ca values,  $1.3 \times 10^{-3} \le Ca \le 20$ , were examined to investigate the effect of stiffness on the stress distribution of the tree for  $\lambda_A = 2.0, 2.6$ , and 3.0 while keeping all other parameters constant at their nominal values. When  $\lambda_A = 2.0$ , a consistent reduction of maximum stress is found from level 1 to 7, as shown in figure 10(a). This is associated with a faster reduction of the cross sections with the branching level. Only for very flexible trees with

 $Ca \gtrsim 10$  is the stress distribution majorly affected by the flexibility. In this case, the tree has improved reconfiguration capability and is able to achieve a lower stress distribution inside all branches. On the other hand, for stiff cases with  $Ca \lesssim 2$ , the location of the maximum stress is always at the stem. This reiterates our previous finding that natural selection might drive tree species with such branching patterns to become more flexible with a good reconfiguration capability or have a stronger trunk for maximum survival.

The case with  $\lambda_A = 2.6$ , as seen in figure 10(b), has a different stress distribution, and over an extensive range of Ca, the tree attains similar stress levels in most of its height. When  $0.25 \le Ca \le 1$ , the stress level remains constant in the lower half of the tree while it shows a slight decrease toward the terminal branches in the upper half. On the other hand, the reconfiguration-dominant response is now shifted to  $Ca \gtrsim 2$ , wherein higher branches deform while the lower part of the tree, including the trunk, preserves its initial configuration. Such a geometrical reconfiguration pattern prompts a uniform stress condition in mid-height while there is a localized stress increase in the trunk and a lower stress level in the terminal branches. Also, by increasing  $\lambda_A$  to 3, the reconfiguration is the critical mechanism. Here for  $Ca \lesssim 1$ , the stress hotspot is placed in the middle of the tree at level 4, with no elevated stress at the trunk as the cross-sectional area of protruding branches decreases fast, and the branches undergo

large deflection through the height. Moreover, as previously explained, in this case, the stress level in the top branches remains high, making the pruning of the top branches the likely damage modes in harsh storms [20]. The deformation pattern of large Ca is shown in figures 10(d)-(f). Large Ca cases show more global deformation from the stem to top branches while the increase of  $\lambda_A$  results in anisotropic deformability with the deflection of upper branches being the dominant feature. The global and local reconfiguration modes of each Ca and  $\lambda_A$  combination regulate the stress distribution in two ways:  $\lambda_A$  modifies the stress distribution through the height and Ca changes the stress magnitude of all branches.

To better study which branching and Cauchy number combinations result in uniform stress through the tree height, we calculate the ratio of over-stress (stress hotspot) magnitude to the mean stress for a range of  $\lambda_A$  and Ca (figure 11). When the lower branching levels of 1-4 are considered, the minimum variation occurs for  $\lambda_A = 2.4-2.8$  at small Ca and only increases to slightly higher values at higher Ca, as shown in figure 11(a). This confirms that the stress distribution of lower branches is not substantially affected by tree flexibility. With the inclusion of more levels, higher sensitivity of the stress variation to Ca is observed. In figure 11(b), for the whole tree length (level 1-7), the minimum stress variation is similar to the first four levels when  $Ca \leq 0.5$ , but it differs for more flexible cases where the optimal conditions switch to higher  $\lambda_A$ . The optimal condition corresponds to a balanced local and global deflection of the tree. Surprisingly, the flexibility and branching ratio marginally affect the stress distribution in the top branches (as shown for levels 5-7 in figure 11(c)), suggesting that the terminal branches themselves do not benefit from adjusting their flexibility and the branching ratio and instead their configuration and their deformability will affect the stress distribution of lower branches.

#### 4.3. Effect of geometrical parameters

The simulations described in section 4.1 and 4.2 have all been conducted at fixed geometrical parameters. This section describes the effect of these parameters on the tree deflection and stress distribution. Here, we alter only one parameter while all other parameters are assumed to be similar to their original values. Overall, as will be discussed, it is found that the other parameters are less important compared to  $\lambda_A$  and Ca.

*Trunkslendernessratio* ( $D_{\rm T}/L_{\rm T}$ ). The trunk's slenderness can affect the response of the tree structure when subjected to gravity and aerodynamic forces. Figure 12 shows how the total maximum stress of branches changes with  $0.1 \leqslant D_{\rm T}/L_{\rm T} \leqslant 0.8$  for three representative  $\lambda_{\rm A}$  values. Overall, a similar decreasing trend in maximum stress with level is

observed for all  $\lambda_A$  cases. The reduction rate of stress, however, is more significant for lower  $\lambda_A$ . It is observed that there is a certain  $D_{\rm T}/L_{\rm T}$  threshold for higher  $\lambda_A$  cases (e.g., 0.2 for  $\lambda_A = 2.6$  and 0.3 for  $\lambda = 3$ ) below which the stress remains very uniform in all branches due to the tree reconfiguration. For all  $\lambda_{\rm A}$  cases, when  $D_{\rm T}/L_{\rm T} > 0.5$ , even though  $\sigma$  is small, large deflection of the top branches results in a fast stress reduction towards the terminal branches. Comparing the deformation pattern of the tree for these cases (figures 12(d)–(f)), it is evident that  $D_{\rm T}/L_{\rm T}$  only modifies the magnitude of the deflection while the reconfiguration pattern remains similar. Overall, for biological relevant slenderness ratio of  $D_{\rm T}/L_{\rm T} \leq 0.5$ , we found that the optimal branching does not change.

Branchinglengthratio ( $\lambda_L$ ). The length ratio of the tree is another fractal parameter that could influence the stress distribution. With all other parameters constant and  $D_T/L_T = 0.3$ , Ca = 0.66, the tree length is varied from  $0.4 \leqslant \lambda_L \leqslant$  1.0. Here, for example,  $\lambda_L = 0.5$  means the length of the mother branch is twice that of a protruding daughter branch, and this relation holds throughout the self-similar tree structure. At the optimal branching ratio of  $\lambda_A = 2.6$ , as seen in figure 13(a), the tree experiences similar stress characteristics for a wide range of  $\lambda_L$  ( $\lambda_L > 0.5$ ). This region is associated with the optimal reconfigurability of the tree structure and the elimination of localized hot stress-bearing spots. This also includes the range of observed  $\lambda_L$  in nature. However, a modified response is observed at small  $\lambda_L$  in which the tree hardly reconfigures and a potential wind-driven breakage is more probable at the trunk.

Branchingangle  $(\gamma)$ . Another parameter that influences the geometry pattern of a branched tree is the self-similar branching angle between daughter branches at each joint. Here, the angle between two daughter branches is varied between  $45^{\circ} \leqslant \gamma \leqslant 105^{\circ}$ , while all other parameters are kept constant. This parameter has a much weaker effect on the stress distribution than other geometrical parameters discussed above. When  $\lambda_{\rm A}=2.6$ , there is only a small local dependency of  $\sigma$  at the trunk to  $\gamma$  (figure 13(b)), and the stress distribution in the tree is almost independent of  $\gamma$ .

#### 4.4. Effect of gravity

Previous studies [42, 84–86] have shown that trees' growth patterns mitigate gravity-induced stresses, enabling them to remain upright and prevent buckling. Other studies, however, suggest that during large bending deflection, when the natural tree posture has been significantly altered, additional gravity-induced stresses contribute to the total stress distribution in trees [73–76, 82]. Here, we show the importance of gravity-induced stresses with tree deflection under extreme wind conditions. It is also discussed that the

prestress stress due to weight (static loading) is negligible compared to wind-induced stresses for rigid and flexible trees and the gravity load only becomes critical for highly reconfigurable trees.

Figure 14 shows the effect of gravity in trees with large deformation for different Ca and  $\lambda_A$ . All other parameters are kept at their nominal values. Here, three types of stress are shown through the tree height: (1) total stress, including both gravity and wind forces  $(\sigma)$ ; (2) total stress without static loading  $(\sigma_{np})$  i.e., only the changes of the gravity stress during the tree deformation are considered (no prestress gravity force); (3) wind-induced stress with zero gravity effect  $(\sigma_{\rm w})$ . When  $Ca = 0.000\,13$  (stiff case),  $\sigma_{\rm np}$  and  $\sigma_{\rm w}$ have similar values suggesting that gravity effects are negligible for stiff trees (figure 14(a)). For all Ca, and  $\lambda_{\rm A}$ ,  $\sigma$  follows the same trend as  $\sigma_{\rm np}$  with a slight decrease in value, this implies that the static loading of the tree due to its weight plays a minimal role in the total stress distribution. Also, when only aerodynamic force is considered and the tree is flexible,  $\sigma_{\rm w}$  is considerably lower but follows the same trend as  $\sigma$ as shown in figure 14(b). The difference in  $\sigma$  and  $\sigma_{\rm w}$ is due to gravity stresses and primarily the gravity load changes during tree deflection  $\sigma_{np}$ . At lower  $\lambda_{\rm A}$ , a global deformation occurs through the tree height, which results in high  $\sigma_{np}$  at all tree levels. As  $\lambda_A$  increases, more local deformation occurs at the top branches and consequently higher  $\sigma_{np}$  at top levels. This gravity action results in  $\sigma$  becoming more uniform when  $\lambda_A = 2.6$ , and exhibiting higher local  $\sigma$  at top branches when  $\lambda_A = 3.0$ .

The effect of gravity is shown in figure 15 for varying Fr between 1 and 30 and the optimal branching of  $\lambda_A=2.6$ . It is found that for all Fr cases, the tree experiences its lowest  $\sigma$  at levels 1 and 2, followed by an increase in level 3, where the branching starts. After level 3, the deformation of top branches and the redistribution of gravity forces induce larger moments on the joints and as a result  $\sigma$  remains approximately constant or only showing a minor increase after level 3. As Fr increases, the tree experiences less gravity force, and the overall gravity-induced stress linearly reduces with an increase in Fr (figure 15). We find that Fr does not significantly impact the stress distribution trend in the tree with the optimal branching ratio.

#### 5. Conclusions

This study examines trees subjected to wind-induced stresses for different branching ratios, Cauchy numbers, and slenderness ratios. The tree is modeled as a self-similar fractal geometry with flexible joints and rigid links exposed to a uniform incoming wind velocity of a magnitude similar to a category three hurricane. We also assume constant stiffness within the tree structure and neglect the effect of leaves on the tree dynamics. The nonlinear equation of motion of the tree is solved to find the modeled tree's

reconfigured shape under combined wind and gravity forces.

For all parameters examined, we find that the branching ratio is the most important factor in determining the stress orientation in rigid and moderately flexible trees. When  $\lambda_A \leq 2.2$ , the tree does not reconfigure to redistribute its stresses among all branches; instead, the maximum stress hotspot is always located at the tree trunk. As  $\lambda$  increases and the diameter of protruding branches from the mother branch further reduces, there is substantial stress redistribution between branches. Progressive deflection in the tree causes the stress to become uniform through the height; thereby, the tree preserves its structural integrity without having localized stress hotspots that could lead to localized breakage. It is observed that trees attain uniform stress distribution at an optimal branching ratio,  $\lambda_A = 2.6$ . At higher  $\lambda_A$ , there is a large deflection in the top branches. As a result, the weight of deflected branches induces significant bending moment, modifying the overall tree stress distribution. This consequently results in an overstress at the top branches.

At the optimal branching,  $\lambda_A = 2.6$ , flexibility only becomes a determining factor in the stress distribution for very flexible trees (Ca > 2). Here, the tree deflection is significant at the trunk, and excessive global deflection from the trunk to the top branches creates localized overstressed regions. The changes of the branches' length through the height is the second factor in determining the stress distribution in the tree. It is observed that at  $\lambda_L > 0.5$ , the tree experiences optimal reconfiguration and eliminates localized stress hotspots, while at  $\lambda_L < 0.5$ , the tree loses its reconfiguration ability, and a region of overstress is always located at the trunk. The angle between two emerging daughter branches at a junction is also weakly tied to the overall stress distribution of the tree, with the stress independent of  $\gamma$  for most cases. Finally, the role of gravity force is investigated, and it is shown that the gravity effects are negligible for trees with limited reconfigurability. Moreover, the static gravity prestress condition of a tree without wind action does not alter the stress patterns in branches for all flexibility levels and branching ratios. However, the change of gravity forces and moments with tree deflection can substantially contribute to the tree's overstressed condition, especially when the tree has large lateral deflection.

The  $\lambda_A$  and  $\lambda_L$  ranges simulated here are consistent with what is observed in natural trees. However, these results can only approximate the resiliency of plant canopies in harsh storms. The optimal parameters may vary slightly for naturally occurring trees (with leaves, anisotropic branch stiffness, and other variations in the tree geometry) subjected to the turbulent atmospheric boundary layer. When the right type of trees are planted next to buildings or added to the natural forests as a mitigation plan, they could

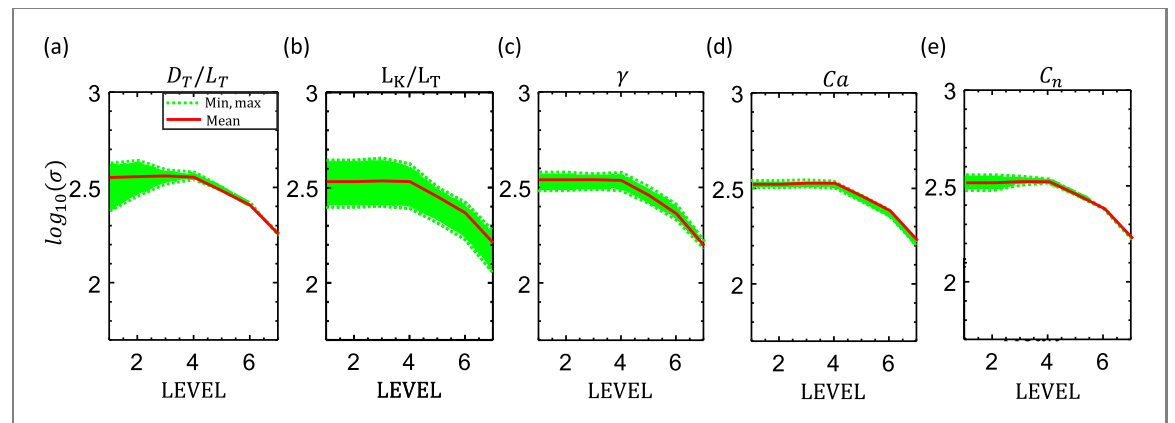


**Figure A1.** Stress magnitude in different levels of the tree for random variations in the tree's geometrical (a)  $D_T/L_T$ , (b)  $L_K/L_T$ , and (c)  $\gamma$ , and structural (d) Ca, and (e)  $C_n$  parameters from the tree trunk to foliage branch when  $\lambda_A = 2.6$ .

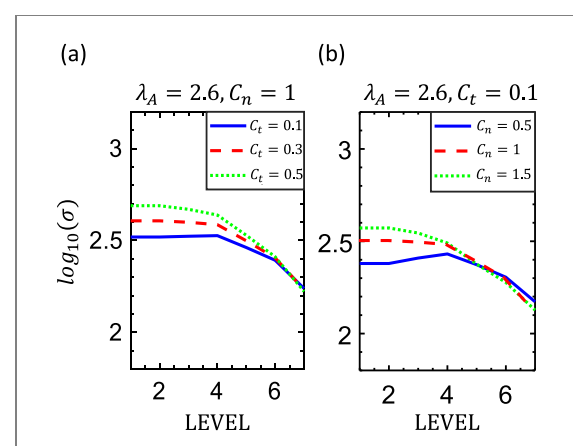


**Figure B1.** Effect of drag coefficients on the total stress  $(\sigma)$  in different tree levels when  $\lambda_A=2.6$  and Ca=0.66 for (a)  $C_t=0.1,0.3,0.5$ , and  $C_n=1$ , and (b)  $C_n=0.5,1,1.5$ , and  $C_t=0.1$ .

act as a shield, preventing excessive damage, just like mangrove forests protect the coast from wave erosion. The selection of optimal shape and flexibility in trees through their long evolution is a multifaceted and complex problem. However, our study suggests that there could be a connection between the shape of trees, their flexibility, and the solution they adopt to survive harsh wind forces. This study can be further broadened to discern tree effects on the flow field and how the tree shapes and flexibility influence the wind-induced damage propagation inside canopies.

## **Funding**

This work is supported by the National Science Foundation, Grant No. CBET-1943810.

#### Acknowledgments

The authors acknowledge NSF-XSEDE for the computational resources through the CTS200043 project on which these simulations were carried out.

# Data availability statement

All data that support the findings of this study are included within the article (and any supplementary files).

# Appendix A. Sensitivity to the variations in geometrical and structural parameters

Here we explore how random changes in the geometrical and structural parameters influence the overall stress distribution in the tree. Each parameter is randomly varied within 15% of the original value from the tree trunk to the foliage branch, while other parameters are kept fixed at their nominal values. In this discussion, we assume  $\lambda_A = 2.6$  for all cases. Forty different random realizations are simulated for each case and their mean values are reported. It is observed that random changes in the branch diameter significantly affect the stress distribution in lower branches and have no effect on higher branches, as shown in figure A1(a). Also, the maximum stress hotspots vary from the tree trunk to the mid-section of the tree, which can influence the location of tree breakage. Random changes in the branch length, Cauchy number, the angle between branches, and drag coefficient do not change the stress distribution in the tree, as shown in figures A1(b)–(e). However, such random variations influence the stress magnitude from the trunk to the foliage branch. A more significant variation in stress magnitude is observed for random variation of branch lengths, while the stress changes are minimal for other parameters. It is also observed that the average stress (uniform from levels 1–4) is almost the same for all cases. Overall, random changes in most geometrical and structural parameters have little effect on the overall stress orientation in the tree.

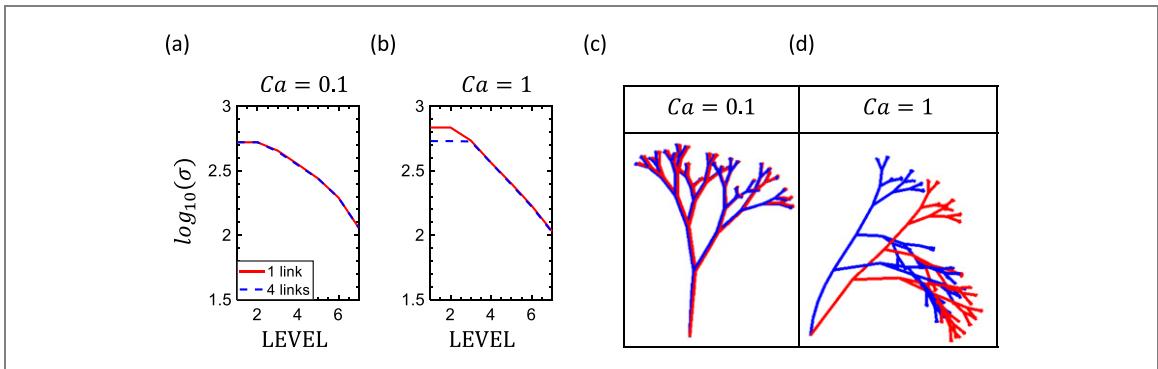


**Figure C1.** Effect of discretization of the tree trunk with four links on the total stress ( $\sigma$ ) in different tree levels when (a) Ca = 0.1 and (b) Ca = 1 and deflection shape when (c) Ca = 0.1 and (d) Ca = 1 for  $\lambda_A = 2.0$ .

## Appendix B. Effect of drag coefficients

Here, the normal and tangential drag coefficients are varied while other parameters are kept at their nominal values. Also,  $D_{\rm T}/L_{\rm T}=0.3$ , Ca=0.66, and  $\lambda_{\rm A}=2.6$ . It is observed that changes in the drag coefficients do not significantly modify the overall stress distribution in the tree, as shown in figures B1(a) and (b). However, the overall magnitude of stress increases with increasing drag coefficients (figure A1 (a) and (b)).

# Appendix C. Effect of discretization of tree branches with multiple links

This appendix investigates the use of multiple links in the tree trunk to study the deformation pattern and stress profile of discretized tree branches. The tree model discussed before is modified to include four links in the tree trunk. It is observed that the total stress and overall tree deflection of the four-link trunk match that of the single link in the small deformation limit (e.g.,  $Ca = 0.1, \lambda_A = 2.0$ ) as shown in figures C1(a) and (c). However, for flexible trees (e.g.,  $Ca = 0.1, \lambda_A = 2.0$ ), the tree deflection and total stress vary slightly in the tree trunk as the singlelink model deflects more than the four-link trunk, as shown in figures C1(b) and (d). This is consistent with our validation of the multi-link system (section 3.3), where adding more links yields less deflection and a slightly more accurate system. A single-link model is used in this study as it is found that with only one link per branch, it would be possible to closely capture the large-scale deformation pattern of the tree and identify the stress profile trend through the tree height.

#### **ORCID** iDs

2810-0065

# References

- [1] Gardiner B, Berry P and Moulia B 2016 Review: wind impacts on plant growth, mechanics and damage *Plant Sci.* **245** 94–118
- [2] Burgess A J et al 2016 The four-dimensional plant: effects of wind-induced canopy movement on light fluctuations and photosynthesis Front. Plant Sci. 7 1392
- [3] de Langre E 2008 Effects of wind on plants *Annu. Rev. Fluid Mech.* **40** 141–68
- [4] Seth M K 2003 Trees and their economic importance *Bot*. Rev. 69 321–76
- [5] Tadrist L, Saudreau M, Hémon P, Amandolese X, Marquier A, Leclercq T and de Langre E 2018 Foliage motion under wind, from leaf flutter to branch buffeting J. R. Soc. Interface 15 20180010
- [6] Kuparinen A 2006 Mechanistic models for wind dispersal Trends Plant Sci. 11 296–301
- [7] David T, Greene D F, Urzay J and Ackerman J D 2014 Turbulence-induced resonance vibrations cause pollen release in wind-pollinated *Plantago lanceolata* L. (*Plantaginaceae*) J. R. Soc. Interface 11 20140866
- [8] Vogel S 2009 Leaves in the lowest and highest winds: temperature, force and shape *New Phytol.* 183 13–26
- [9] Schuepp P H 1972 Studies of forced-convection heat and mass transfer of fluttering realistic leaf models *Bound.-Layer Meteorol.* 2 263–74
- [10] Grace J 1978 The turbulent boundary layer over a flapping Populus leaf Plant Cell Environ. 1 35–8
- [11] Defraeye T, Herremans E, Verboven P, Carmeliet J and Nicolai B 2012 Convective heat and mass exchange at surfaces of horticultural products: a microscale CFD modelling approach Agric. For. Meteorol. 162–163 71–84
- [12] Roden J S and Pearcy R W 1993 Effect of leaf flutter on the light environment of poplars Oecologia 93 201-7
- [13] Roden J S and Pearcy R W 1993 Photosynthetic gas exchange response of poplars to steady-state and dynamic light environments *Oecologia* 93 208–14
- [14] Melese Endalew A, Debaer C, Rutten N, Vercammen J, Delele M A, Ramon H, Nicolaï B M and Verboven P 2011 Modelling the effect of tree foliage on sprayer airflow in orchards *Bound.-Layer Meteorol.* 138 139–62
- [15] Gilet T and Bourouiba L 2014 Rain-induced ejection of pathogens from leaves: revisiting the hypothesis of splash-on-film using high-speed visualization *Integr. Comp. Biol.* 54 974–84
- [16] Yamazaki K 2011 Gone with the wind: trembling leaves may deter herbivory Biol. J. Linn. Soc. 104 738–47
- [17] Warren J 2015 Is wind-mediated passive leaf movement an effective form of herbivore defence? *Plant Ecol. Evol.* 148 52–6

- [18] National Centers for Environmental Information (NCEI) 2019 Billion-dollar weather and climate disasters: overview https://ncdc.noaa.gov/billions/
- [19] Dorfman J H, Liu Y and Rabinowitz A N 2018 Estimating agricultural losses from a hurricane J. Agribus. 36 199–206
- [20] Lopez D, Michelin S and de Langre E 2011 Flow-induced pruning of branched systems and brittle reconfiguration *J. Theor. Biol.* 284 117–24
- [21] Mayer H 1987 Wind-induced tree sways Trees 1 195-206
- [22] Moulia B, Coutand C and Lenne C 2006 Posture control and skeletal mechanical acclimation in terrestrial plants: implications for mechanical modeling of plant architecture Am. J. Bot. 93 1477–89
- [23] Metzger K 1893 Der Wind als maßgebender Faktor für das Wachsthum der Bäume Mündener Forstliche Hefte 5 35–86
- [24] Mattheck C 1990 Engineering components grow like trees Mater.wiss. Werkst.tech. 21 143–68
- [25] Niklas K J and Spatz H-C 2000 Wind-induced stresses in cherry trees: evidence against the hypothesis of constant stress levels *Trees* 14 230–7
- [26] Niklas K J 2000 Computing factors of safety against wind-induced tree stem damage J. Exp. Bot. 51 797–806
- [27] Lawton R O 1982 Wind stress and elfin stature in a montane rain forest tree: an adaptive explanation Am. J. Bot. 69 1224–30
- [28] Milne R and Blackburn P 1989 The elasticity and vertical distribution of stress within stems of *Picea sitchensis Tree Physiol*, 5 195–205
- [29] Lopez D, Eloy C, Michelin S and de Langre E 2014 Drag reduction, from bending to pruning *Europhys. Lett.* 108 48002
- [30] Duryea M L and Kampf E 2007 Wind and trees: lessons learned from hurricanes *EDIS* 2007 1–17
- [31] Hedden R L, Fredericksen T S and Williams S A 1995 Modeling the effect of crown shedding and streamlining on the survival of loblolly pine exposed to acute wind Can. J. For. Res. 25 704–12
- [32] da Vinci L 1955 Notebooks ed E ed MacCurdy (New York: Braziller)
- [33] Eloy C 2011 Leonardo's rule, self-similarity, and wind-induced stresses in trees Phys. Rev. Lett. 107 258101
- [34] James K R, Haritos N and Ades P K 2006 Mechanical stability of trees under dynamic loads *Am. J. Bot.* 93 1522–30
- [35] Bertram J E 1989 Size-dependent differential scaling in branches: the mechanical design of trees revisited *Trees* 3
- [36] Murray C D 1927 A relationship between circumference and weight in trees and its bearing on branching angles J. Gen. Physiol. 10 725–9
- [37] Kruszewski P and Whitesides S 1998 A general random combinatorial model of botanical trees J. Theor. Biol. 191 221–36
- [38] Zhi W, Ming Z and Qi-xing Y 2001 Modeling of branching structures of plants I. Theor. Biol. 209 383–94
- [39] Minamino R and Tateno M 2014 Tree branching: Leonardo da Vinci's rule versus biomechanical models *PLoS One* 9
- [40] Oppelt A L, Kurth W and Godbold D L 2001 Topology, scaling relations and Leonardo's rule in root systems from African tree species *Tree Physiol.* 21 117–28
- [41] Vogel S 1984 Drag and flexibility in sessile organisms Am. Zool. 24 37–44
- [42] McMahon T A and Kronauer R E 1976 Tree structures: deducing the principle of mechanical design J. Theor. Biol. 59 443–66
- [43] Koehl M A R 1984 How do benthic organisms withstand moving water? Am. Zool. 24 57–70
- [44] Kane B, Pavlis M, Harris J R and Seiler J R 2008 Crown reconfiguration and trunk stress in deciduous trees Can. J. For. Res. 38 1275–89

- [45] Alben S, Shelley M and Zhang J 2002 Drag reduction through self-similar bending of a flexible body *Nature* 420 479–81
- [46] Gosselin F, de Langre E and Machado-Almeida B A 2010 Drag reduction of flexible plates by reconfiguration *J. Fluid Mech.* 650 319–41
- [47] Moore J R and Maguire D A 2004 Natural sway frequencies and damping ratios of trees: concepts, review and synthesis of previous studies *Trees* 18 195–203
- [48] Spatz H-C, Brüchert F and Pfisterer J 2007 Multiple resonance damping or how do trees escape dangerously large oscillations? Am. J. Bot. 94 1603–11
- [49] Sellier D, Brunet Y and Fourcaud T 2008 A numerical model of tree aerodynamic response to a turbulent airflow Forestry 81 279–97
- [50] Milne R 1991 Dynamics of swaying of Picea sitchensis Tree Physiol. 9 383–99
- [51] Miller L A 2005 Structural dynamics and resonance in plants with nonlinear stiffness J. Theor. Biol. 234 511–24
- [52] Theckes B, de Langre E and Boutillon X 2011 Damping by branching: a bioinspiration from trees *Bioinsp. Biomim.* 6 046010
- [53] Murphy K D and Rudnicki M 2012 A physics-based link model for tree vibrations Am. J. Bot. 99 1918–29
- [54] Finnigan J J and Mulhearn P J 1978 Modelling waving crops in a wind tunnel Bound.-Layer Meteorol. 14 253–77
- [55] Spatz H-C and Speck O 2002 Oscillation frequencies of tapered plant stems Am. J. Bot. 89 1–11
- [56] Brüchert F, Speck O and Spatz H-C 2003 Oscillations of plants' stems and their damping: theory and experimentation *Phil. Trans. R. Soc.* B 358 1487–92
- [57] Sellier D, Fourcaud T and Lac P 2006 A finite element model for investigating effects of aerial architecture on tree oscillations *Tree Physiol.* 26 799–806
- [58] Sellier D and Fourcaud T 2009 Crown structure and wood properties: influence on tree sway and response to high winds Am. J. Bot. 96 885–96
- [59] Dupuy L X, Fourcaud T, Lac P and Stokes A 2007 A generic 3D finite element model of tree anchorage integrating soil mechanics and real root system architecture Am. J. Bot. 94 1506–14
- [60] Rodriguez M, de Langre E and Moulia B 2008 A scaling law for the effects of architecture and allometry on tree vibration modes suggests a biological tuning to modal compartmentalization Am. J. Bot. 95 1523–37
- [61] James K, Dahle G, Grabosky J, Kane B and Detter A 2014 Tree biomechanics literature review: dynamics Arboric. Urban For. 40 1–15
- [62] Chester S, Meneveau C and Parlange M B 2007 Modeling turbulent flow over fractal trees with renormalized numerical simulation J. Comput. Phys. 225 427–48
- [63] Bentley L P, Stegen J C, Savage V M, Smith D D, von Allmen E I, Sperry J S, Reich P B and Enquist B J 2013 An empirical assessment of tree branching networks and implications for plant allometric scaling models *Ecol. Lett.* 16 1069–78
- [64] Torab P and Piovesan D 2016 Vibrations of fractal structures: on the nonlinearities of damping by branching J. Nanotechnol. Eng. Med. 6 034502
- [65] Ellison A M and Niklas K J 1988 Branching patterns of Salicornia europaea (Chenopodiaceae) at different successional stages: a comparison of theoretical and real plants Am. J. Bot. 75 501–12
- [66] Leopold L B 1971 Trees and streams: the efficiency of branching patterns J. Theor. Biol. 31 339–54
- [67] Siciliano B, Sciavicco L, Villani L and Oriolo G 2009 Robotics: Modelling, Planning and Control (Berlin: Springer)
- [68] Shabana A A 2013 Dynamics of Multibody Systems (Cambridge: Cambridge University Press)
- [69] Hahn H 2002 Rigid Body Dynamics of Mechanisms: 1 Theoretical Basis (Berlin: Springer)
- [70] Li C-J and Sankar T S 1993 Systematic methods for efficient modeling and dynamics computation of flexible robot manipulators *IEEE Trans. Syst. Man Cybern. Syst.* 23 77–95

- [71] Ayachour E H 2003 A fast implementation for GMRES method J. Comput. Appl. Math. 159 269–83
- [72] Pernice M and Walker H F 1998 NITSOL: a Newton iterative solver for nonlinear systems SIAM J. Sci. Comput. 19 302–18
- [73] Jones H G 2013 Plants and Microclimate: A Quantitative Approach to Environmental Plant Physiology (Cambridge: Cambridge University Press)
- [74] Peltola H M 2006 Mechanical stability of trees under static loads Am. J. Bot. 93 1501–11
- [75] Peltola H and Kellomäki S 1993 A mechanistic model for calculating windthrow and stem breakage of Scots pines at stand age Silva Fenn. 27 99–111
- [76] Petty J A and Swain C 1985 Factors influencing stem breakage of conifers in high winds Forestry 58 75–84
- [77] Ehrenstein U and Eloy C 2013 Skin friction on a moving wall and its implications for swimming animals *J. Fluid Mech.* 718 321–46
- [78] Taylor G I 1952 Analysis of the swimming of long and narrow animals *Proc. R. Soc.* A **214** 158–83
- [79] Wang J, McKinley P K and Tan X 2014 Dynamic modeling of robotic fish with a base-actuated flexible tail J. Dyn. Syst. Meas. Control 137 011004

- [80] Banerjee A K and Nagarajan S 1997 Efficient simulation of large overall motion of beams undergoing large deflection Multibody Syst. Dyn. 1 113–26
- [81] Virot E, Ponomarenko A, Dehandschoewercker É, Quéré D and Clanet C 2016 Critical wind speed at which trees break Phys. Rev. E 93 023001
- [82] Gardiner B, Peltola H and Kellomäki S 2000 Comparison of two models for predicting the critical wind speeds required to damage coniferous trees *Ecol. Model.* 129 1–23
- [83] Ryan M G and Yoder B J 1997 Hydraulic limits to tree height and tree growth BioScience 47 235–42
- [84] Alméras T and Fournier M 2009 Biomechanical design and long-term stability of trees: morphological and wood traits involved in the balance between weight increase and the gravitropic reaction *J. Theor. Biol.* 256 370–81
- [85] McMahon T 1973 Size and shape in biology: elastic criteria impose limits on biological proportions, and consequently on metabolic rates *Science* 179 1201–4
- [86] Fournier M, Bailleres H and Chanson B 1994 Tree biomechanics: growth, cumulative prestresses, and reorientations *Biomimetics* 2 229–51